Journal of Crystal Growth 593 (2022) 126781

Contents lists available at ScienceDirect

Journal of Crystal Growth

journal homepage: www.elsevier.com/locate/jcrysgro

Luminescence and Raman spectroscopic properties of cubic boron nitride grown by drop-casting technique

Mohammad Mahafuzur Rahaman [a], Shantanu Saha [b], Syed M.N. Hasan [b], Weicheng You [b], Arnob Ghosh [b], Md Saiful Islam Sumon [b], S.K. Shafaat Saud Nikor [b], Benjamin Freeman [b], Shrivatch Sankar [b], Hendrik Colijn [c], Sharif Md. Sadaf [d], Jivtesh Garg [e], Shamsul Arafin [b,*]

[a] Department of Materials Science and Engineering, The Ohio State University, Columbus, OH 43210, USA
[b] Department of Electrical and Computer Engineering, The Ohio State University, Columbus, OH 43210, USA
[c] Centre for Electron Microscopy and Analysis, The Ohio State University, Columbus, OH 43210, USA
[d] Institut National De La Recherche Scientifique (INRS), Varennes, QC, Canada
[e] School of Aerospace and Mechanical Engineering, University of Oklahoma, Norman, OK 73019, USA

ARTICLE INFO

Keywords:
A1. Characterization
A1. Defects
A1. Point defects
A3. High resolution X-ray diffraction
B1. Nanomaterials
B2. Semiconducting III-V materials

ABSTRACT

The emission of sub-bandgap photons from a ultrawide bandgap cubic-boron nitride material is a phenomenon that can be applied to next-generation quantum photonic devices. This paper reports the structural and morphological characteristics of this new research material synthesized by the drop-casting technique in ambient conditions. Our x-ray diffraction (XRD) analysis shows a primary peak at ~44° related to the (111) plane which confirms the cubic phase of boron nitride. The optical and vibrational properties of the material were investigated by cathodoluminescence and Raman spectroscopic measurements, respectively. The optical study provides experimental evidence of four different radiative sub-bandgap levels in the visible spectral region. These preliminary findings show a potential route to implement high-performance quantum emitters using this highly-sought material with extreme properties.

1. Introduction

Cubic-boron nitride (c-BN), an analog of diamond, is the second hardest material (33--45 GPa) in the world [1,2]. This indirect wide bandgap material (E_g ~ 6.4 eV) with a low dielectric constant (7.1) and high breakdown field (>15 MV/cm) also has the second-best thermal conductivity after diamond [3–6]. While the scientific community is still struggling to achieve quality *n*-type diamond, c-BN can be doped both *p*- and *n*-types unlike hexagonal boron nitride (h-BN) [3,7,8]. Moreover, c-BN also surpassed diamond in thermal and chemical stability [9]. This is also an excellent material for high-temperature, high breakdown field and high-power electronic devices operating in harsh environments than that envisioned for diamond films [4]. Hence, this material with extreme properties has been proven to be good for radio frequency (RF) and power electronics. Due to its high emission efficiency at deep ultraviolet wavelengths, this is also considered as a promising optoelectronic material [10].

Beyond electronics and classical optoelectronics, this functional wide bandgap material has gained tremendous attention as a "quantum" material as it can host atomic defects and provide the resulting single photon emitters [11]. In other words, the presence of optically addressable quantum emitters originating from the point defects in c-BN renders this material useful for quantum applications [11]. Defects in c-BN can potentially reduce the bandgap and produce different sub-bandgap levels. The point defect-induced sub-bandgap emission/absorption feature serves as color centers, making c-BN an excellent source for quantum correlated photon emitters [12]. Among many point defects, neutral oxygen-vacancy defects in c-BN showed potential towards achieving a scalable platform for realization of quantum information processing, qubit, sensing and beyond [13]. Defect complexes such as boron vacancy (V_B)-substitutional oxygen (O_N) (i.e. V_BO_N center) is a plausible qubit candidate in *p*-type c-BN [13]. Native and extrinsic defects in c-BN suggested the presence of oxygen-related defects with isoelectronic properties similar to nitrogen vacancy (NV-) centers in diamond [14].

Since the earliest report on synthesis and characterization in the

* Corresponding author.
E-mail address: arafin.1@osu.edu (S. Arafin).

https://doi.org/10.1016/j.jcrysgro.2022.126781
Received 18 May 2022; Received in revised form 23 June 2022; Accepted 24 June 2022
Available online 27 June 2022

early 1960s [15], c-BN has been studied and characterized on the material level with the goal of achieving classical and quantum emitters. Compared to h-BN, experimental demonstrations of optical quantum emission from the native and extrinsic point defects of c-BN are, however, elusive. Comprehensive research to identify the sub-bandgap excitations/emissions of c-BN, which are the origin of radiative emissions, is also rare in the literature. Very recently, observation of room-temperature single photon emission from c-BN was reported which showed spans of zero phonon lines (ZPLs) covering a wide range (496 nm–700 nm) of the visible region [11]. Interestingly, obtaining BN with the pure cubic phase through a robust growth technique is challenging and often the as-grown material yields small fractions of h-BN [16,17], impacting material properties significantly.

Successful utilization of this novel material on the targeted quantum applications requires intellectual understanding of this material, placing an unprecedented demand for systematic characterization and the subsequent in-depth analysis. Motivated by the presence of point defects in c-BN and the recent work on isolated individual defects that emit single photons, the simple drop-cast technique was used to synthesize c-BN on SiO_2-coated silicon substrates and the material was then subsequently characterized by microscopic and spectroscopic measurements. Our systematic and detailed experimental study of c-BN using multi-wavelength Raman and room-temperature cathodoluminescence (CL) measurements reveal the dominant nature of transverse optical (TO) and longitudinal optical (LO) phonon peaks and deep-level defect emission from c-BN. This study also identifies the presence of hexagonal phase within the optically probed regions of nanocrystalline c-BN. Our analysis reveals somewhat phase impurity in c-BN and identifies the sub-bandgap defect levels responsible for deep emission in the visible range.

2. Experimental details

2.1. Synthesis

Nanopowder of c-BN from PlasmaChem GmbH was first dispersed in deionized (DI) water and drop-casted onto a SiO_2/Si substrate. The c-BN powder used in the study has purity >99% with a specific surface area of >11 m^2/g. The average particle size of the powder is 165 nm with a full range of 80–450 nm. Although achieving large-area and uniform thickness films are desired to study the material properties, drop-casting is not a great technique to achieve continuous and uniform thickness of synthesized materials. However, the simple drop-cast technique can quickly provide materials on any substrates, does not require any expensive growth process, and allows one to achieve a large signal during characterization study due to thick materials obtained from the synthesis process. Prior to drop-casting c-BN, 300 nm thick SiO_2 was deposited on silicon substrates using plasma enhanced chemical vapor deposition (PECVD). When it comes to choosing DI water vs ethanol, one considers three major points that include fast evaporation rate, strong surface tension, and strong capillary force. Due to a high vapor pressure, using solvents are better than water since they evaporate much faster. However, as soon as we drop solvent with suspended nanopowder on substrates, it spreads out very quickly and end up with large-area and non-uniform c-BN flakes. Therefore, water was used as solvent in this study since it has enriched surface tension and capillary force, which will restrain the c-BN within a small surface area on the SiO_2/Si substrate during our drop-casting process, resulting in the formation of characterization c-BN nanocrystals. The sample was then heated at 100 °C in ambient for 20 mins. Since we are using SiO_2-coated substrates resulting a hydrophilic surface, i.e. good wettability was achieved by using DI water.

The sample preparation steps, and the schematic view of the drop-casted c-BN on SiO_2-coated Si substrates are shown in Fig. 1(a) and (b). The drop-casted sample shows the coffee-ring effect at the edge of the droplet as displayed in Fig. 1(c). The coffee ring effect is driven by the interplay between microscopic fluid flow in the droplet and the rate at which it evaporates. The edge of the droplets covers larger free space due to which the evaporation water flux near the edge is greater than that at the center, which leads to water along with c--BN flowing towards the edge. Contact pinning line formed by surface tension restricts further spreading of the solvent. As a result, particle accumulation at the dry film boundaries is accelerated, and a coffee ring is formed [18]. These accumulated particles slowdown the spread of the boundaries and confine the c-BN within smaller area on SiO_2, resulting in evolution of thick c-BN. The width of the ring was, thus, found to be 250 μm − 300 μm which indicates that the major fraction of the area within the coffee ring follows the same pattern in the formation of c-BN.

2.2. Characterization of c-BN

A scanning electron microscope (SEM) with a Zeiss Ultra Plus standard detector was used to examine the morphology of the c-BN. X-ray

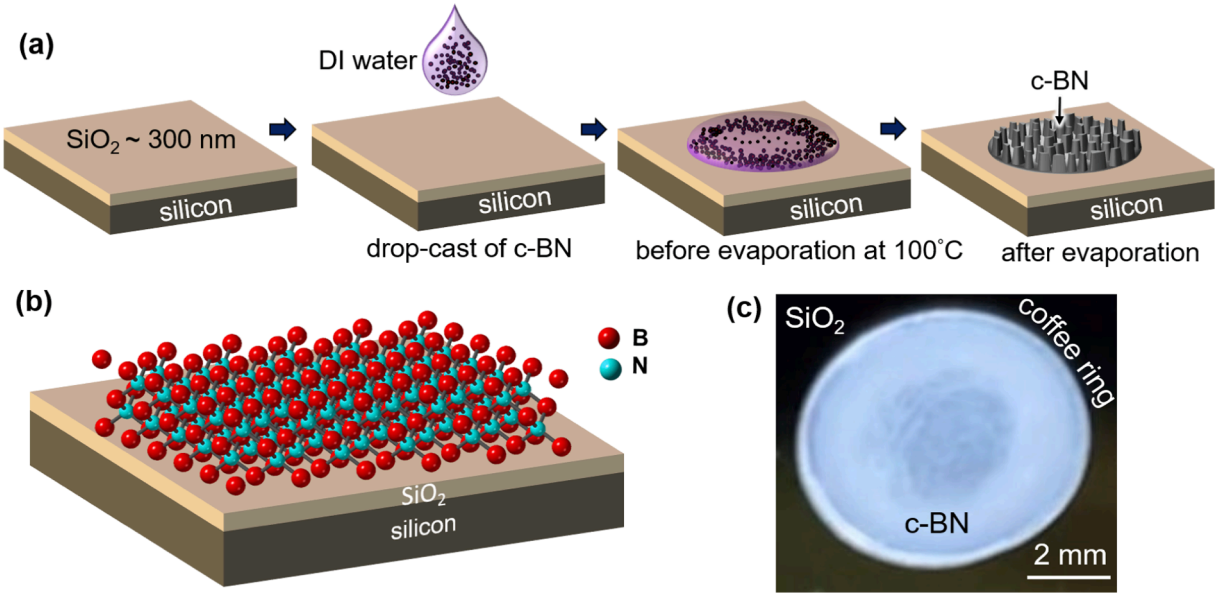

Fig. 1. (a) Preparation of drop-casted c-BN on SiO_2/Si substrates, (b) schematic view of c-BN with the atomic geometry, and (c) optical microscopic image of c-BN.

diffraction (XRD) measurements were performed on a Rigaku rotating anode system equipped with a Cu-targeted anode (operated at 40 kV and 200 mA), monochromator, and scintillation detector. Parallel beam thin-film optics were employed with the theta drive locked at an alpha angle of 0.25°. The samples were analyzed in a digital step scan mode from 20° to 80°. Raman measurements were carried out under a N_2 atmosphere in a Linkam stage using a Renishaw in Via system. An accumulation of 20 scans, each of 30-s duration, was collected using 250 μW 488 nm, 514 nm and 632 nm excitation sources, 20 μm slits, and a 3000 lines/mm grating for each measurement. The CL measurements were carried out by a Horiba H-Clue detector system integrated with a Thermo Scientific Quattro Environmental SEM. A charge coupled device (CCD) detector was used in CL measurements. The accelerating voltage and the probe current were varied at 10 kV, 15 kV, and 20 kV and 0.29 nA, 0.34 nA, and 0.40 nA, respectively, to inspect the c-BN material at different depths.

3. Results and discussions

Fig. 2(a) shows the top-view SEM image of the drop-casted c-BN nanocrystals. The nanoparticles in the droplet have greater surface tension due to their higher surface area to volume ratio. While drop-casting using a pipette, nanoparticles minimize surface free energy by forming a neck-like network with their neighbors, reducing the total potential energy and surface area. As surface coverage increases and surface tension decreases, coalescence of particles becomes difficult at one stage where micrometer-sized particles form. A coalescence of the nanoscale-size powder to few tens of micrometer ranges is seen. The process takes place at lower temperatures when coalescence is slower, resulting in irregular shape agglomeration [19]. Thus, the surface of drop-casted c-BN contains unevenly distribution of agglomerated particles, as shown in Fig. 2(a) and in the final step of schematic Fig. 1(a). The dimensions of agglomerated particles calculated from SEM images are around 37 μm.

The quantitative analysis of the c-BN sample was performed by energy dispersive spectroscopy (EDS). The result of EDS spectra is shown in Fig. 2(b); this confirms the significant presence of B and N. The stoichiometric composition of the material was confirmed by calculating the B/N ratio which was found to be 0.96. The peaks of C, O, Na, Si, S, and Cl also appeared in the spectra which may have originated from the substrate or the ambient during deposition. Similar presence of impurities in the drop-cast technique performed in ambient was also reported [20].

The structure of the drop-casted c-BN was performed by XRD measurements. The XRD pattern of c-BN nanocrystals is shown in Fig. 3. The cubic nature of BN was found by the dominant (111)-peak appearing at

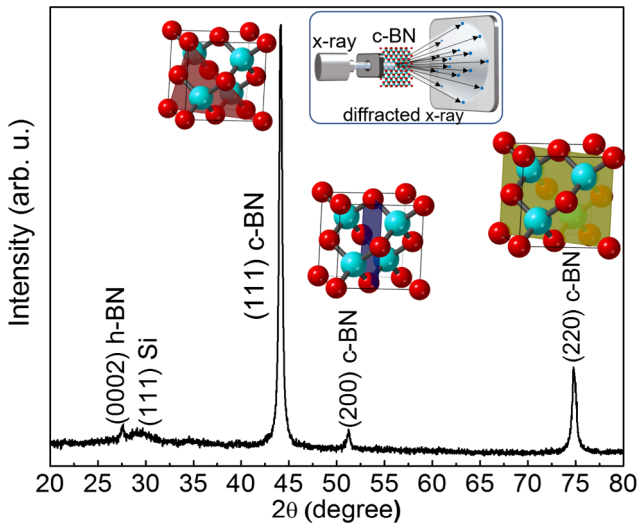

Fig. 3. XRD spectra of drop-casted c-BN.

44.1°. The full width at half maximum (FWHM) value of the (111) peak was measured to be 0.34°, and the resulting average crystallite size c-BN was calculated as 4.3 nm which is smaller than reported values [19]. The measured c-axis lattice constant was 3.55 Å, which is close to the bulk c-BN value of 3.61 Å [21]. The decrease in lattice constant may be attributed to the contraction of lattice due to higher surface area in nanomaterials as well as the local residual strain which is probably due to variations in the crystallize size of the nano-powder. Two more diffraction peaks of c-BN were revealed at 51.2° and 74.8°, known as the (200) and (220) peaks, respectively [22,23]. In fact, (111) diffraction peaks should be the dominant one that suggests the cubic nature of c-BN. The measured peak ratio of (220) to (111) is about 0.22 which is much larger than the value of randomly oriented c-BN, i.e., 0.06 [23]. This implies that the c-BN crystallites are mostly oriented along the (111) plane with the presence of fewer crystallites within the (220) plane. Hence, a measured ratio of 0.22 in our work justifies that the c-BN nanocrystals have a preferential orientation along the (111) plane. The atomic geometry of the (111), (200) and (220) planes of c-BN are also presented in Fig. 3. As three cubic phases of different crystallite sizes are present in the c-BN nanocrystals, their orientation difference may generate strain in our c-BN. Two extra peaks, (0002) of h-BN and (111) of Si substrates were also identified in the spectra. The intensity of (0002) peak is insignificant compared to the intensity of (111) peak of c-BN which confirms that the amount of h-BN present in the drop-casted c-

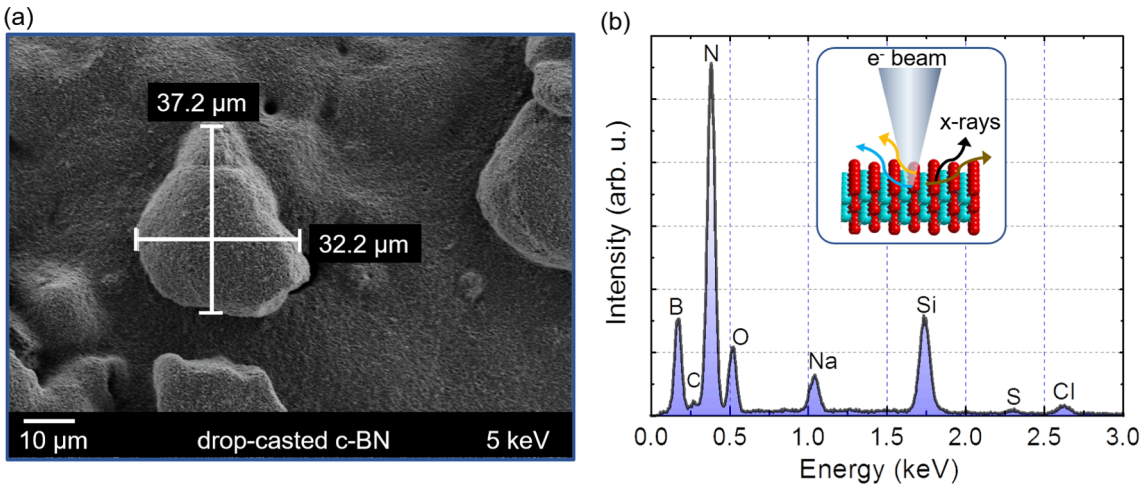

Fig. 2. (a) SEM image of agglomerated c-BN and (b) its EDS spectra.

BN is negligible.

In order to identify the chemical structure, phase and polymorphs of the drop-cast sample, Raman spectroscopy was conducted. A well-resolved Raman spectrum of c-BN is presented in Fig. 4. The spectrum shows two Lorentzian-shaped TO- and LO-phonon peaks of c-BN at 1041 cm^{-1} and 1249 cm^{-1}, respectively, when excited by a 514 nm laser [24]. Both TO- and LO- Raman peaks exhibit slightly asymmetric lineshapes. Given a symmetric, sharp peak is observed in the case of crystalline material centered at frequency corresponding to the zone centered phonon frequency, poor crystallinity of our c-BN can be estimated. While the TO peak was found to be narrower, the LO peak was broader. With respect to single crystal c-BN, the observed asymmetric and broader LO peak could be tentatively attributed to the phonon confinement effect as a result of the existence of micro- or nanocrystals of c-BN. The phonon modes of our c-BN are shifted with respect to the bulk modes at 1054 and 1306 cm^{-1}, suggesting a residual compressive stress in our c-BN. This stress is likely to be induced during the c-BN synthesis process. The downshifted LO peak shift from the bulk c-BN could also be due to the different crystallite size of the c-BN nanopowder used in our study. Similar phenomena have been reported earlier for c-BN [25,26], justifying the peak shifts in our sample. The FWHM of the intense TO peak was 18 cm^{-1} which is close to the reported value for c-BN films grown by the CVD technique [24]. The calculated spectral lineshape of the LO peak is 81 cm^{-1} which is more than two orders of magnitude broader than the reported value [26]. Such LO broadening as also reported in [27], could be attributed to the presence of nano-crystallites and a high defect concentrations in our c-BN samples.

To get further insights on our material under study, multiwavelength Raman measurements were carried out using non-resonant 488 nm, 514 nm, and 632 nm excitations. Compared with the previous Raman measurement, a different position of the c-BN sample was probed while performing multiwavelength Raman. The resulting spectra are shown in Fig. 5. Excitation by multiple wavelengths allows the enhancement of weak Raman peaks by breaking Raman selection rules and activating forbidden and/or inactive modes that can be used to identify real energy band transitions in materials [28]. The TO peak appears at 1039 cm^{-1}, which is shifted by 7 and 11 cm^{-1} towards lower energies when excited by 488 nm and 632 nm, respectively. On the other hand, the LO peak of 514 and 632 nm excitation emerge at 1256 cm^{-1}. This peak shifts to 1280 cm^{-1} when excited by the 488 nm laser. The presence of local strain and thickness variation in the drop-casted c-BN could be the primary reason for this shift. Phase segregation of c-BN could also occur during the synthesis process of c-BN nanopowder. A doubly degenerate E_{2g} peak of h-BN is also observed at the downshifted energies with respect to the bulk signature peak of h-BN at ~ 1366 cm^{-1}. The h-BN phase was observed at all these three excitation wavelengths which indicates that the drop-casted sample contains some amount of h-BN phase. The position of the peak is consistent with the reported value for the LO phase of h-BN [29]. The reduced intensity of this peak in comparison to the TO and LO peak intensities of c-BN indicates that the amount of h-BN phase is trivial. Further optimization of the c-BN synthesis process is necessary to completely remove the hexagonal phase.

The sub-bandgap level emission in the c-BN was detected by performing CL measurements. Room temperature CL spectra of c-BN recorded at 10, 15, and 20 kV electron energies are presented in Fig. 6. The CL spectra primarily reveal four different peaks within the visible range. Peak shifting is not observed with altering the irradiated electron energies due to the absence of other polymorphs in the sample. Four emission peaks centered at about 2.04, 2.40, 3.1, and 3.67 eV were observed. The emission peak at ~2.04 eV is close to those previously

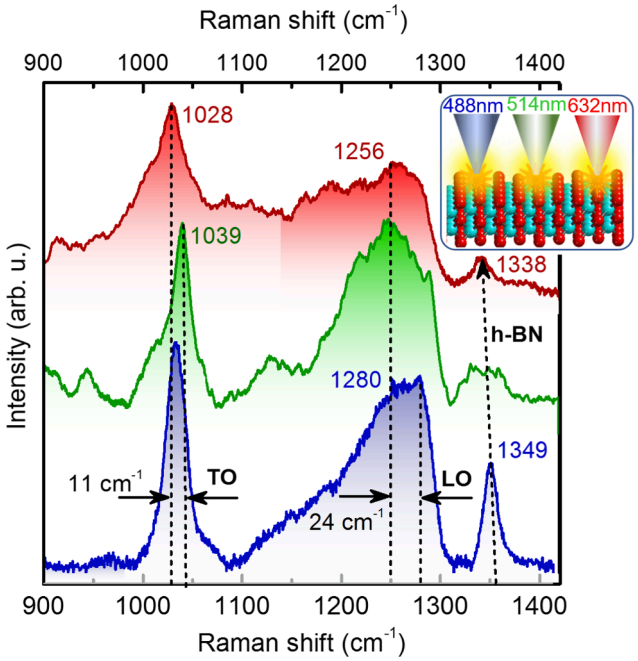

Fig. 5. Raman spectra of drop-casted c-BN using different wavelength excitation.

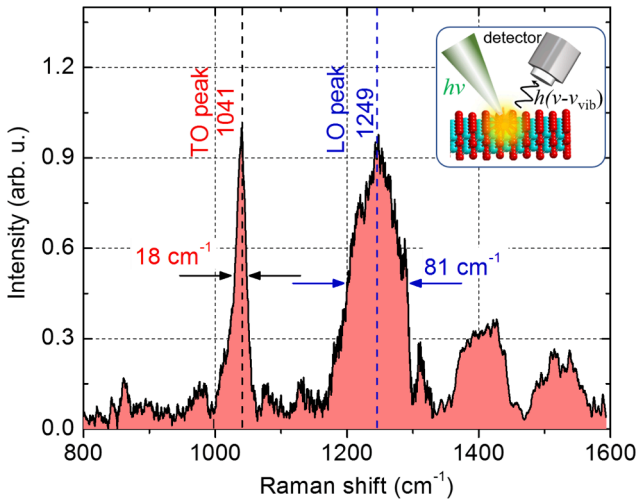

Fig. 4. Raman spectra of drop-casted c-BN performed by 514 nm wavelength.

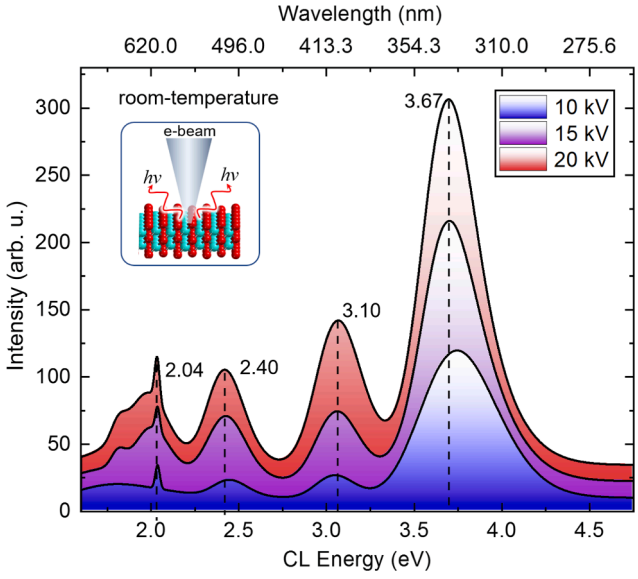

Fig. 6. Room temperature CL spectra of c-BN at different electron energies.

reported at ~1.97 eV and ~2.08 eV obtained at room temperature from c-BN prepared by drop-cast and CVD techniques, respectively [11,17]. It is considered as a typical peak from c-BN. This emission peak was not, however, observed in Refs. [30,31]. The origin of this CL peak is not yet fully understood. The next peak is found at 2.4 eV with a FWHM of around 175 meV. This peak is reported in Refs. [11,32] which could be originated from an emission band at around 2.48 eV of c-BN due to the boron and NV-based multivacancy complexes related to Frenkel pair defects [30]. Such intrinsic complex defects within CVD-grown diamond were found to be responsible for emission of ZPL, a key signature for single photon emission [14]. The peak at 3.1 eV could be tentatively attributed to the presence of nitrogen vacancies in c-BN [33]. The peak was reported from undoped c--BN crystal which could be a signal from the UCL band or US-1 or GB-1 center [32,34]. The presence of such NVs is promising for implementing high-performance solid-state quantum emitters. The distinctive properties of this peak such as long coherence times of electron and nuclear spin states, spin-state initialization, single photon emission make it highly desirable for quantum applications. A broad emission from deep-level defects at 3.67 eV is observed in the sample. An emission center close to this peak around 3.5 eV was reported for c-BN thin films grown by RF sputtering [35]. The same peak at around 3.6 eV was also reported in Refs. [31,36]. It is speculated that this peak could arise from the PF1 center of c-BN [31].

4. Conclusion

In summary, the drop-cast technique was employed to synthesize c-BN in ambient conditions which was then characterized by SEM, EDS, XRD, Raman, and CL measurements. Although the experimental characterization techniques employed here constitute a regular identification procedure, our thorough investigation revealed some valuable insights on the structural, vibration and optical properties of c-BN. The SEM images show that the surface was covered with micron-sized irregularly shaped c-BN agglomerates. The c-BN sample has a cubic structure with preferred orientation along (111), as confirmed by XRD. The Raman and multiwavelength Raman measurements confirm that the amount of h-BN phase present in the c-BN sample is insignificant. The four sub-bandgap level emissions within the visible region determined by CL study provide a picture of defect luminescence of c-BN and confirms that the optical signatures of some of the observed defects resemble the previously reported ones. Although the chemical nature of the point defects causing the sub-bandgap emission is not identified, this preliminary study will aid future endeavors to find their origin which will in turn expedite the process of developing single photon emitters from specific point defects of c-BN for next-generation quantum photonics.

5. Author statement

Mohammad Mahafuzur Rahaman: Material Synthesis, Original draft preparation. **Shantanu Saha**: Material Characterization, Original draft preparation. **Syed M N Hasan:** Material Characterization. **Weicheng You:** Material Characterization. **Arnob Ghosh:** Reviewing and Editing. **Md Saiful Islam Sumon:** Reviewing and Editing. **SK Shafaat Saud Nikor:** Proofreading and Editing. **Benjamin Freeman:** Material Synthesis. **Shrivatch Sankar:** Material Characterization, Reviewing and Editing. **Hendrik Colijn:** Material Characterization. **Sharif Md Sadaf**: Reviewing and Editing. **Jivtesh Garg:** Reviewing and Editing. **Shamsul Arafin**: Conceptualization, Writing- Reviewing and Editing.

Declaration of Competing Interest

The authors declare that they have no known competing financial interests or personal relationships that could have appeared to influence the work reported in this paper.

Acknowledgements

We thank the anonymous reviewers for their time in giving useful comments and suggestions, which have improved the contents of the manuscript.

This work was supported in part by The Ohio State University Materials Research Seed Grant Program, funded by the Center for Emergent Materials, an NSF-MRSEC, grant DMR1420451, the Center for Exploration of Novel Complex Materials, and the Institute for Materials Research. Electron microscopy was performed at the Center for Electron Microscopy and Analysis (CEMAS) at The Ohio State University.

References

[1] M. Ohring, Interdiffusion, reactions, and transformations in thin films, in: M. Ohring (Ed.), Materials Science of Thin Films (Second Edition), Chapter 11, Academic Press, San Diego, 2002, pp. 641–710.
[2] S.N. Monteiro, A.L.D. Skury, M.G. de Azevedo, G.S. Bobrovnitchii, Cubic boron nitride competing with diamond as a superhard engineering material–an overview, J. Mater. Res. Technol. 2 (1) (2013) 68–74.
[3] A. Soltani, A. Talbi, V. Mortet, A. BenMoussa, W.J. Zhang, J.C. Gerbedoen, J.C. De Jaeger, A. Gokarna, K. Haenen, P. Wagner, G. Ferro, P. Siffert, Diamond and cubic boron nitride: properties, growth and applications, AIP Conf. Proc. 1292 (1) (2010) 191–196.
[4] K. Hirama, Y. Taniyasu, H. Yamamoto, K.J.A.P.L. Kumakura, Control of n-type electrical conductivity for cubic boron nitride (c-BN) epitaxial layers by Si doping, Appl. Phys. Lett. 116 (16) (2020), 162104.
[5] N. Izyumskaya, D.O. Demchenko, S. Das, Ü. Özgür, V. Avrutin, H. Morkoç, Recent development of boron nitride towards electronic applications, Adv. Electron. Mater. 3 (5) (2017) 1600485.
[6] X. Zhang, Doping and electrical properties of cubic boron nitride thin films: a critical review, Thin Solid Films 544 (2013) 2–12.
[7] M.E. Turiansky, D. Wickramaratne, J.L. Lyons, C.G.V.d. Walle, Prospects for n-type conductivity in cubic boron nitride, Appl. Phys. Lett. 119(16) (2021) 162105.
[8] K. Nose, H. Yang, T. Yoshida, Electrical characterization of p-type cubic boron nitride/n-type silicon heterojunction diodes, Diam. Relat. Mater. 14 (8) (2005) 1297–1301.
[9] Y. M. Chong, "PhD thesis," City University of Hong Kong, Hong Kong, 2009.
[10] O. Mishima, K. Era, J. Tanaka, S. Yamaoka, Ultraviolet light-emitting diode of a cubic boron nitride PN junction made at high pressure, Appl. Phys. Lett. 53 (11) (1988) 962–964.
[11] G.I. López-Morales, A. Almanakly, S. Satapathy, N.V. Proscia, H. Jayakumar, V. N. Khabashesku, P.M. Ajayan, C.A. Meriles, V.M. Menon, Room-temperature single photon emitters in cubic boron nitride nanocrystals, Opt. Mater. Express 10 (4) (2020) 843–849.
[12] A. Tararan, S. di Sabatino, M. Gatti, T. Taniguchi, K. Watanabe, L. Reining, L.H. G. Tizei, M. Kociak, A. Zobelli, Optical gap and optically active intragap defects in cubic BN, Phys. Rev. B 98 (9) (2018), 094106.
[13] G. Bian, H. Yuan, N. Zhang, L. Xu, J. Zhang, P. Fan, H. Wang, C. Zhang, G. Shan, Q. Zhang, J. Fang, Neutral oxygen-vacancy defect in cubic boron nitride: a plausible qubit candidate, Appl. Phys. Lett. 114 (10) (2019), 102105.
[14] T.A. Abtew, W. Gao, X. Gao, Y. Sun, S. Zhang, P. Zhang, Theory of oxygen-boron vacancy defect in cubic boron nitride: a diamond NV− isoelectronic center, Phys. Rev. Lett. 113 (13) (2014), 136401.
[15] R.H. Wentorf Jr., Preparation of semiconducting cubic boron nitride, J. Chem. Phys. 36 (8) (1962) 1990–1991.
[16] Z.-P. Su, Y.-H. Du, X.-R. Ji, D.-P. Yi, X.-X. Yang, X.-L. Gong, T.-C. Zhang, Synthesis of cubic boron nitride by the reaction of Li_3N and B_2O_3, Chin. Phys. Lett. 23 (8) (2006) 2285–2287.
[17] J. Yu, C. Ong, Y. Wong, M. Lau, S. Matsumoto, Morphology dependence of cathodoluminescence from cubic boron nitride films deposited by chemical vapor deposition, J. Appl. Phys. 99 (12) (2006), 124915.
[18] A. Kaliyaraj Selva Kumar, Y. Zhang, D. Li, G. Compton, A mini-review: How reliable is the drop casting technique? Electrochemistry Communications 121 (2020) 106867.
[19] T. Hawa, R. Zachariah, Coalescence kinetics of unequal sized nanoparticles, J. Aerosol Sci. 37 (1) (2006) 1–15.
[20] M. Nagamine, M. Osial, W.-Kalinowska, K. Jackowska, and P. Krysiński, Photosensitive thin films based on drop cast and Langmuir-Blodgett hydrophilic and hydrophobic CdS nanoparticles, Nanomaterials 10(12) (2020) 2437.
[21] V. Solozhenko, V. Chernyshev, G. Fetisov, V. Rybakov, I. Petrusha, Structure analysis of the cubic boron nitride crystals, J. Phys. Chem. Solids 51 (8) (1990) 1011–1012.
[22] S. Matsumoto, W. Zhang, High-rate deposition of high-quality, thick cubic boron nitride films by bias-assisted DC jet plasma chemical vapor deposition, Jpn. J. Appl. Phys. 39 (5B) (2000) L442–L444.
[23] Y.-P. Guo, Z.-Z. Song, G.-C. Li, G.-H. Chen, Growth of preferentially oriented cubic boron nitride films by chemical vapor deposition, Acta Physica Sinica 5 (2) (1996) 143–150.
[24] J. Zhang, S. Matsumoto, Investigations of crystallinity and residual stress of cubic boron nitride films by Raman spectroscopy, Phys. Rev. B 63 (7) (2001), 073201.

[25] W. Sun, Y. Wang, Y. Ko, Raman spectroscopy of single nanodiamond: Phonon-confinement effects, Appl. Phys. Lett. 92 (15) (2008), 153115.
[26] O. Kutsay, C. Yan, M. Chong, Q. Ye, I. Bello, J. Zhang, A. Zapien, F. Zhou, K. Li, V. Garashchenko, G. Gontar, V. Novikov, T. Lee, Studying cubic boron nitride by Raman and infrared spectroscopies, Diam. Relat. Mater. 19 (2010) 968–971.
[27] H. Herchen, A. Cappelli, Temperature dependence of the cubic boron nitride Raman lines, Phys. Rev. B 47 (21) (1993) 14193–14199.
[28] M. Placidi, M. Dimitrievska, V. Izquierdo-Roca, X. Fontané, A. Castellanos-Gomez, A. Pérez-Tomás, N. Mestres, M. Espindola-Rodriguez, S. López-Marino, M. Neuschitzer, V. Bermudez, A. Yaremko, A. Pérez-Rodríguez, Multiwavelength excitation Raman scattering analysis of bulk and two-dimensional MoS2: vibrational properties of atomically thin MoS2 layers, 2D Materials 2 (3) (2015), 035006.
[29] R.J. Nemanich, S.A. Solin, R.M. Martin, Light scattering study of boron nitride microcrystals, Phys. Rev. B 23 (12) (1981) 6348–6356.
[30] R. Cossio, F. Fizzotti, E. Vittone, A.L. Giudice, C. Manfredotti, S. Nistor, Low temperature CL investigation of BN1 vibronic structure in c-BN, Diamond Related Materials 15 (2006) 1166–1168.
[31] C. Manfredotti, R. Cossio, A.L. Giudice, E. Vittone, F.J.P.R.B. Fizzotti, Vibronic spectrum of c-BN measured with cathodoluminescence, Phys. Rev. B 74 (15) (2006), 155204.
[32] J. Zhang, H. Kanda, S. Matsumoto, Cathodoluminescence of cubic boron nitride films deposited by chemical vapor deposition, Appl. Phys. Lett. 81 (18) (2002) 3356–3358.
[33] Y. Kumashiro, Electric Refractory Materials, CRC Press, New York, 2000.
[34] E.M. Shishonok, Luminescence centers in cubic boron nitride, J. Appl. Spectrosc. 74 (2) (2007) 272–277.
[35] C.A. Taylor, S.W. Brown, V. Subramaniam, S. Kidner, S.C. Rand, R. Clarke, Observation of near-band-gap luminescence from boron nitride films, Appl. Phys. Lett. 65 (10) (1994) 1251–1253.
[36] D. Evans, A.G. McGlynn, B.M. Towlson, M. Gunn, D. Jones, T.E. Jenkins, R. Winter, N. Poolton, Determination of the optical band-gap energy of cubic and hexagonal boron nitride using luminescence excitation spectroscopy, J. Phys.: Condens. Matter 20 (7) (2008), 075233.